The Madden–Julian Oscillation, Barotropic Dynamics, and North Pacific Tropical Cyclone Formation. Part II: Stochastic Barotropic Modeling

DENNIS L. HARTMANN AND ERIC D. MALONEY

Department of Atmospheric Sciences, University of Washington, Seattle, Washington

(Manuscript received 20 September 2000, in final form 9 February 2001)

ABSTRACT

A stochastic barotropic model linearized about the 850-mb flow is used to investigate the relationship between wind variations associated with the Madden–Julian oscillation (MJO) and eddy kinetic energy variations in the Tropics. Such a model is successful in predicting the observed location of eddy kinetic energy maxima during the westerly phase of the MJO and the suppression of eddy activity during the easterly phase of the MJO. The concentration of eddy energy during the westerly phase results from the strong east–west and north–south gradients of the large-scale wind fields. The model shows that barotropic wave propagation and wave mean–flow interaction tend to concentrate small-scale Rossby wave energy in regions of convergence, which may be an important mechanism for organizing convection into tropical cyclones. The structure and barotropic energetics of the wave activity are similar to those observed, but the modeled eddies are smaller in scale and do not move westward as do the observed eddies. The eddies that dominate the observed correlations are heavily modified by convection, but barotropic processes can explain the localization of eddy energy by the MJO that is observed.

1. Introduction

Maloney and Hartmann (2000, hereafter MH00) showed that the extension of the Madden–Julian oscillation (MJO) into the eastern Pacific Ocean strongly modulates the occurrence of tropical storms there. Liebmann et al. (1994) showed a similar modulation of tropical cyclones by the MJO in the western Pacific. In Part I (Maloney and Hartmann 2001), we use National Centers for Environmental Prediction (NCEP) reanalysis data to show that barotropic energy conversions modulated by MJO mean flow variations contribute to the focusing of tropical cyclone activity by the MJO. It was shown that the barotropic energy conversions can replace the localized eddy kinetic energy (EKE) maxima in about two days. One might question whether these energy conversions are indirectly dependent on eddy driving by latent heat release, however, since observed statistics are probably dominated by eddies that receive substantial energy from latent heat release. In this study we use a barotropic model linearized about the MJO wind composites at 850 mb to show that the strong energy localization and associated conversions can be simulated in a model with no explicit latent heat release. The modeling presented here underlines the potential importance of the low-level MJO wind variations for focusing eddy energy in regions of tropical storm formation. In the model this focusing is achieved entirely through barotropic processes.

Gray (1998) gives six parameters of the mean climatological conditions that can be used to predict the frequency of tropical cyclone formation. The first three are dynamical—the Coriolis parameter, the low-level relative vorticity, and the inverse of the vertical wind shear—and the last three are thermodynamic: the sea surface temperature, the contrast in equivalent potential temperature between the surface and 500 mb, and the midtropospheric humidity. Zehr (1992) adds low-level convergence and pre-existing disturbances to the list of helpful conditions for tropical cyclone formation. In MH00 and Part I we show that the vorticity, convergence, vertical shear, and stability are all modulated by the MJO in the east Pacific in a manner that according to Gray's (1998) and Zehr's (1992) criteria should lead to the observed modulation of tropical storms by the MJO. Here we focus more specifically on the provision of seed disturbances that can organize tropical convection. Although we consider here only the mature and suppressed phases of the MJO, the provision of energy in rotational disturbances with eastward group velocity may also be important for triggering convection at the leading edge of the MJO, as appears to occur in nature (Nakazawa 1986). The pumping of the boundary layer by vorticity in the free troposphere may be important in initiating convection in regions where a dry lower troposphere inhibits the development of deep convection.

Corresponding author address: Prof. Dennis L. Hartmann, Department of Atmospheric Sciences, University of Washington, Box 351640, Seattle, WA 98195-1640.
E-mail: dennis@atmos.washington.edu

Liebmann et al. (1994) showed that in the western Pacific the MJO modulates the number of tropical cyclones, but that the proportion of cyclones that reach hurricane intensity does not change much. Therefore, provision of seed disturbances may be an important factor in tropical storm formation and a key factor in the modulation of hurricanes by the MJO. Sobel and Bretherton (1999) showed that barotropic energy propagation is an important source of eddy activity in the tropical cyclone formation region of the western Pacific and Sobel and Maloney (2000) used Plumb's wave propagation diagnostic to show that MJO and ENSO variations affect eddy energies there.

In Part I we investigated the variability of synoptic wave energy in the eastern and western Pacific that is associated with MJO-related variations in zonal wind. The MJO variability in the Pacific takes the form of alternating westerly and easterly flow anomalies near the equator. The westerly or positive phase is associated with enhanced tropical cyclone and hurricane activity. In the westerly phase the synoptic eddy kinetic energy is enhanced on the cyclonic and downstream quadrant of the westerly anomalies, very near the region of most frequent formation of tropical depressions. An analysis of the barotropic eddy generation terms at 850 mb shows significant source terms associated with the horizontal gradients of the mean wind field for the positive composite. In the easterly phase of the MJO, the eddy kinetic energy is suppressed. It is hypothesized that the influence of horizontal gradients of the mean wind on barotropic eddy dynamics is an important factor in determining the differences in eddy activity between the westerly and easterly phases of the MJO variations in the Pacific. Analysis of the barotropic dynamics shows that conversion from mean to eddy kinetic energy occurs in exactly the right locations to support the increased eddy kinetic energy in the westerly phase of the MJO. The energy conversions replace the eddy energy in about two days, which is a strong enough source to produce significant energy in the presence of realistic dissipation. This concentration of energy occurs in the region of tropical cyclone genesis.

In this paper, we use a simple stochastic barotropic model to show that we can produce key elements of the differences between the observed westerly and easterly MJO composites of the east and west North Pacific during summer, including the energy conversions and basic wave structure. By focusing on the importance of barotropic dynamics, we do not mean to imply that vertical shear and thermodynamic variables are unimportant. Rather we use a barotropic model to isolate the effect of barotropic influences of the 850-mb flow in determining eddy structure and the distribution of eddy variance. These modeling results support the premise that barotropic vorticity dynamics in the lower troposphere are central to understanding the distribution and structure of tropical eddies that might serve as seed disturbances for tropical cyclones and hurricanes. In the case of the westerly MJO composite, these seed disturbances concentrate where cyclonic low level vorticity, convergence, weak vertical shear, and high SST provide a favorable environment for cyclogenesis. The observational work in Part I and the modeling work described here thus support each other.

The model we use is described in section 2. The model responses to some idealized wind distributions are discussed in section 3. The results for the westerly and easterly MJO composite flow fields in the eastern Pacific are described in section 4, and for the western Pacific in section 5. The results are summarized in section 6.

2. The model

Basic-scale analysis suggests that, away from convection, the dynamics of synoptic-scale disturbances in the Tropics should be essentially barotropic (Charney 1963; Holton 1992). In the Tropics vertical motion is proportional to the diabatic heating rate, and away from convection heating rates are small. Even with modest convection driving more substantial vertical motions, scale analysis suggests that vertical advection of vorticity is less important than horizontal advection in the Tropics. If V, W, L, and H give the horizontal and vertical velocity and length scales, respectively, then the ratio of the vertical to horizontal advection is WL/HV. Choosing $V = 10$ m s^{-1}, $L = 10^6$ m, $H = 10^4$ m, and using a heating rate of 5 K day^{-1}, vertical advection is still a factor of 10 smaller than horizontal advection. Diagnostic studies confirm that vorticity dynamics are barotropic to first order in many situations (Shapiro 1978; Davidson and Hendon 1989; Sobel and Bretherton 1999), although convection appears to play a strong role in the vorticity budget of mature depressions (Reed and Johnson 1974; Stevens 1979).

We hypothesize on the basis of this theory and evidence that a barotropic model may provide a first-order explanation for the modulation of eddy variance in some regions of the Tropics. This hypothesis may be a weak one for disturbances that are very strongly driven by convection, but convective heating is often limited to a small portion of a developing system, so that at any level the structure and dynamics of the storm are still heavily constrained by almost barotropic vorticity dynamics, particularly where strong horizontal wind gradients are present. Also, pre-existing synoptic eddies are often necessary to organize deep convection in the Tropics. So part of our goal here is to see how well a barotropic theory can do in explaining the response of eddy kinetic energy to MJO wind variations. If an adiabatic, barotropic theory correctly predicts the modulation of eddy activity by the MJO, then we may logically conclude that adiabatic barotropic responses to mean wind variations are important, and that the effect of convection is to amplify, rather than to negate, the barotropic effects.

We will show here that a barotropic model linearized

about the mean flow at 850 mb for the MJO composites of Part I can produce differences in synoptic wave activity between the two composites that are similar to observed differences. The spatial scale and movement of the modeled eddies are suitable to organize convection, but the modeled eddies have a smaller spatial scale and less movement than the observed eddies.

A barotropic analysis of realistic flows can be made by looking at linear stochastic perturbations about the two-dimensional time-mean state. The linear operator is made stable by adding a suitable amount of dissipation, and the problem is treated as a Langevin equation forced with random noise. The linear perturbations that have the right structure for the mean wind distribution are favored and dominate the statistics of the resulting stochastic–dynamic problem. This approach has been applied to long barotropic waves in middle latitudes (Gambo 1982; Egger and Schilling 1984; Metz 1987; Newman et al. 1997) and to midlatitude baroclinic waves (Farrell and Ioannou 1994; Whitaker and Sardeshmukh 1998). Penland and Matrosova (1994) have discussed stochastic modeling of ENSO.

In this paper our objective is to use the simplest dynamical model that will illustrate the relationship between variations in the large-scale wind structure and the distribution of eddy kinetic energy with spatial and temporal scales suitable for providing the seed disturbances which can organize tropical convection to produce tropical storms. We will use a barotropic nondivergent model linearized about the time mean flow at 850 mb for this purpose. Part of our hypothesis is that low-level wind variations are paramount, and so we will use the 850-mb flow averaged for different phases of the composite MJO event from our observational work.

Sardeshmukh and Hoskins (1988) have argued that to investigate the vorticity dynamics at a single level in the Tropics it is appropriate to use the nondivergent vorticity equation linearized about the time-mean (divergent) flow. This is the approach we will use in this paper. We have also done all the experiments shown here with a shallow water model with a 240-m equivalent depth as used, for example, by Nieto-Ferreira and Schubert (1997). In the experiments with the shallow-water model the mean flow also had a balanced time-mean geopotential field. For the present problem the shallow water model and the nondivergent model produce very consistent simulations. Since it is difficult to justify the first internal mode analogy of the shallow-water model in an environment with substantial vertical variations in mean wind, we have chosen to show the results for the nondivergent model, which constitutes a consistent approximation for the vorticity balance at a single level.

The governing equation for eddy vorticity ζ' is thus

$$\frac{\partial \zeta'}{\partial t} = -\nabla \cdot (\mathbf{V}_\psi + \mathbf{V}_\chi)\zeta' - \mathbf{v}'_\psi \cdot \nabla(\overline{\zeta} + f) - \alpha\zeta' + k\nabla^4\zeta' + x(t). \quad (1)$$

Where $\mathbf{V}_\psi$ and $\mathbf{V}_\chi$ are the rotational and divergent parts of the mean flow velocity vector, respectively, $\mathbf{v}'_\psi$ is the perturbation rotational wind vector, an overbar indicates time average, and a prime indicates the deviation from the time average. Also included are linear damping at a rate α, and biharmonic diffusion with coefficient k. A linear damping timescale of 5 days is used in all the calculations shown here. This damping makes the flow stable and represents a plausible timescale for damping by surface friction and radiation. The biharmonic diffusion coefficient is chosen to provide a damping timescale of 2 days for the highest resolved wavenumber (T63). The qualitative nature of the results are not sensitive to a doubling or halving of the dissipation parameters. The time mean velocities are the 850-mb wind composites for the westerly and easterly phases of the MJO in the east and west Pacific.

Eddies are driven with red noise forcing of the vorticity equation. The noise forcing at each spatial grid point is constructed from an autoregressive process using the following formula:

$$x(t) = r(\Delta t)x(t - \Delta t) + (1 - r(\Delta t)^2)^{1/2}\varepsilon(t), \quad (2)$$

where $x(t)$ is the noise forcing, and $\varepsilon(t)$ is a Gaussian white noise process with unit variance and zero mean. The parameter $r(\Delta t)$ is the autocorrelation at one time step Δt. The process (2) generates a red noise time series with an exponential autocorrelation function with an e-folding decay time of $T = -\Delta t/\ln[r(\Delta t)]$. We use $T =$ 2 days, but using 1 day or 5 days produces qualitatively similar results. The variance of the linear response tends to increase with increasing persistence of the noise, but the spatial distribution of the noise and its response to the wind distribution are not sensitive to moderately large variations of T, so long as T is not too small. If T is set to zero, then the model response is very weak because the meteorological modes do not have time to respond to the noise forcing variations. The noise is completely uncorrelated in space, so that the noise forcing has no preferred spatial scale, but is autocorrelated in time with a decorrelation time of 2 days. The random forcing thus has a spectrum that is white in space and slightly red in frequency, with no preferred direction of phase propagation. The desired eddy statistics are derived by time integration, using a spherical harmonic transform method (Bourke 1972) with a triangular 63 truncation, so that the highest resolved wavenumber has a wavelength of about 5.7°, or 635 km at the equator.

3. Idealized cases showing the role of convergence and shear

In this section we calculate eddy statistics with the stochastic barotropic model for highly idealized mean wind distributions to illustrate the effects of wind convergence and wind shear. We begin with a simple convergent flow described by a hyperbolic tangent zonal

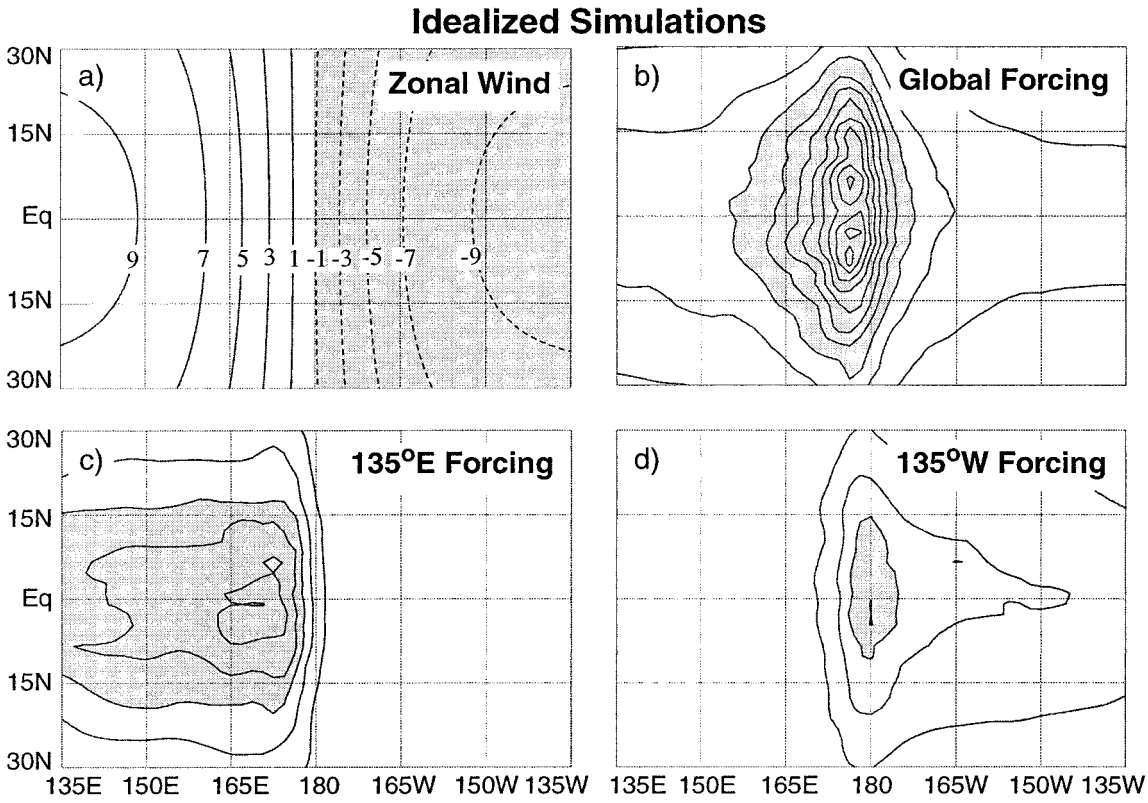

FIG. 1. (a) Idealized zonal wind and associated eddy kinetic energy distributions for (b) zonally uniform noise, (c) noise to west of wind convergence, and (d) noise to east of convergence. Contour interval is 2 m s^{-1} for zonal wind. The contour interval for EKE is 3 m^2 s^{-2} and values greater than 15 m^2 s^{-2} are shaded.

flow variation. The zonal wind is specified to be of the form

$$u(\lambda, \varphi) = U_0 \tanh[(\lambda - \lambda_0)/D] \cos\varphi, \qquad (3)$$

with $U_0 = 10$ m s^{-1} and $D = 20°$. This gives a strong zonal wind convergence at the central longitude λ_0 (Fig. 1a). With this mean wind distribution, the distribution of eddy kinetic energy that results from a zonally uniform noise forcing can be calculated. The noise forcing is independent of longitude, but is constrained by a window function that is Gaussian about the equator, with an *e*-folding width of 30°: $W(\varphi) = \exp[-(\varphi/C)^2]$, where $C = 30°$. Figure 1b shows the resulting eddy kinetic energy in this case, which peaks strongly slightly to the west of the convergence longitude, where the wind goes to zero. The eddy kinetic energy distribution is asymmetrical because Rossby waves are more effectively forced in the westerly winds, and their group velocity is toward the east, where they converge in the weakening westerlies. The response of the stochastic barotropic model is well explained by wave propagation theory (Webster and Chang 1988; Holland 1995; Sobel and Bretherton 1999).

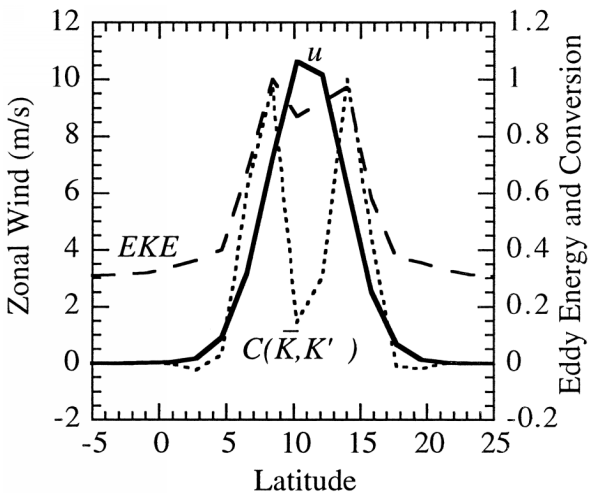

FIG. 2. Mean zonal wind (solid), $C(\overline{K}, K')$ (dotted), and eddy kinetic energy (dashed) for a zonally symmetric jet at 11°N as functions of latitude.

Rossby wave energy accumulates in regions where the westerly winds converge, and particularly strongly where the group velocity goes to zero near a zero wind line (Webster and Chang 1988). One can investigate this further by using a zonally isolated noise forcing. In this case the noise has the same wavenumber and frequency distribution, but it is constrained to occur in a fixed

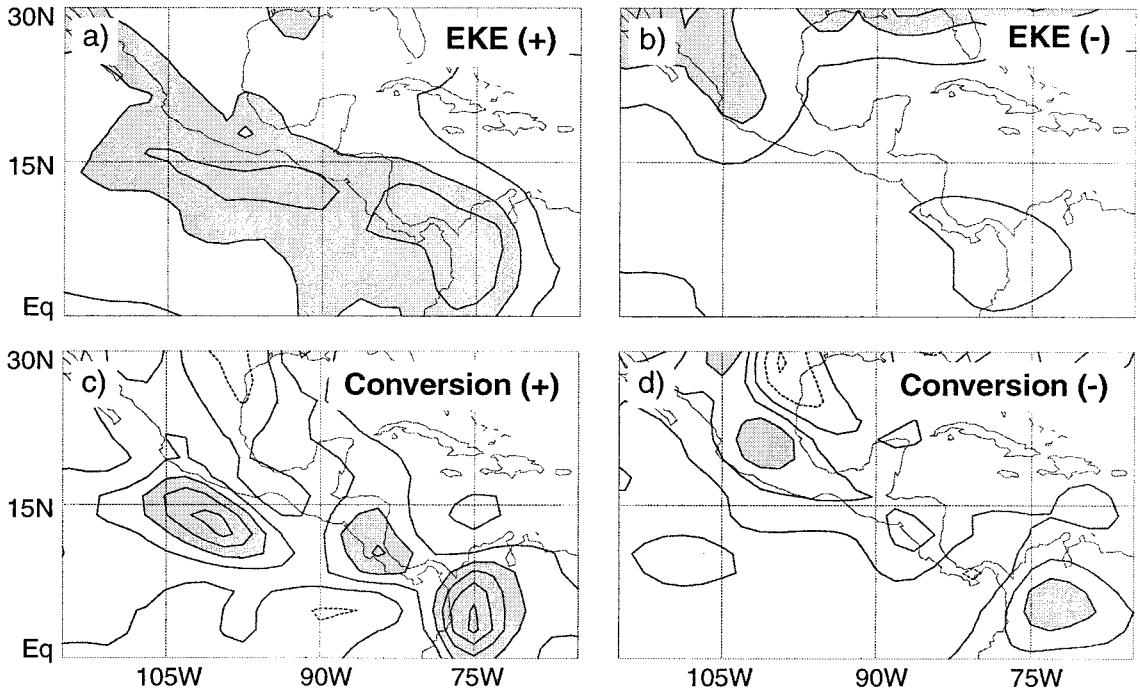

FIG. 3. Simulated 850-mb eddy kinetic energy in the east Pacific for the (a) positive and (b) negative MJO basic states. The contour interval is 3 $m^2\ s^{-2}$ and values greater than 9 $m^2\ s^{-2}$ are shaded. Simulated barotropic conversion from mean to eddy kinetic energy $C(\overline{K}, K')$ for the (c) positive and (d) negative MJO composite wind fields. Contour interval is $2.0 \times 10^{-5}\ m^2\ s^{-3}$, contours greater than $4.0 \times 10^{-5}\ m^2\ s^{-3}$ are shaded. Negative contours are dotted.

geographical region by applying a spatial window of the form

$$W(\lambda, \varphi) = \exp\{-[(\lambda - \lambda_1)/B]^2\} \exp[-(\varphi/C)^2], \quad (4)$$

where $B = 40°$, $C = 30°$, and λ_1 is chosen to put the center of the window 45° to the east or west of the zonal wind reversal. The resulting eddy kinetic energy distributions for noise centered west or east of the wind reversal are shown in Figs. 1c,d, respectively. When the noise is centered in the westerlies to the west of the wind reversal the EKE maximum is larger than when the noise is centered in the easterlies to the east of the wind reversal. This is again because Rossby waves can exist in the westerlies, and their group velocity converges toward the wind reversal. Noise introduced into the westerly side of the wind convergence is thus more effective in producing a strong EKE maximum than is noise introduced into the easterly side of a wind convergence.

Wind anomalies associated with MJO variations often have a strong meridional shears associated with them. The dominant mode of zonal flow variability in the east Pacific (Fig. 1 of Part I) is a narrow jet centered near 11°N. To investigate the effect of this wind structure, we construct an idealized zonal wind distribution that is independent of longitude, but has a Gaussian jet in latitude,

$$u(\varphi) = u_o \exp\{-[(\varphi - \varphi_0)/\Delta\varphi]^2\} \quad (5)$$

where $u_o = 11\ m\ s^{-1}$, $\varphi_0 = 11°N$, and $\Delta\varphi = 4°$. This wind profile is shown in Fig. 2, along with the eddy kinetic energy and the conversion rate from mean to eddy energy. Although the flow profile is stable in the presence of strong dissipation, the energy conversion peaks strongly at the edges of the jet, and the eddy energy peaks there also. So the downgradient transport of momentum can be an important source of eddy energy even when the flow is stable but under the influence of noise forcing (Farrell and Ioannou 1993). In cases with significant meridional shear, the meridional flux of momentum can play a significant role in generating EKE, as indicated in Part I and as will be shown below for the observed MJO wind composites.

4. Simulation of eddy response to observed MJO wind variations: East Pacific

To investigate the barotropic energetics of observed MJO composites, the model is linearized about 850-mb winds derived from NCEP–National Center for Atmospheric Research reanalysis. The positive and negative wind composites for the east Pacific, which are displayed in Fig. 6 of Part I, are used here as the basic state for the model calculations. Our model is global, and we use the global wind analysis in our simulations and apply noise uniformly over the sphere. The response in the regions of interest is only sensitive to the local

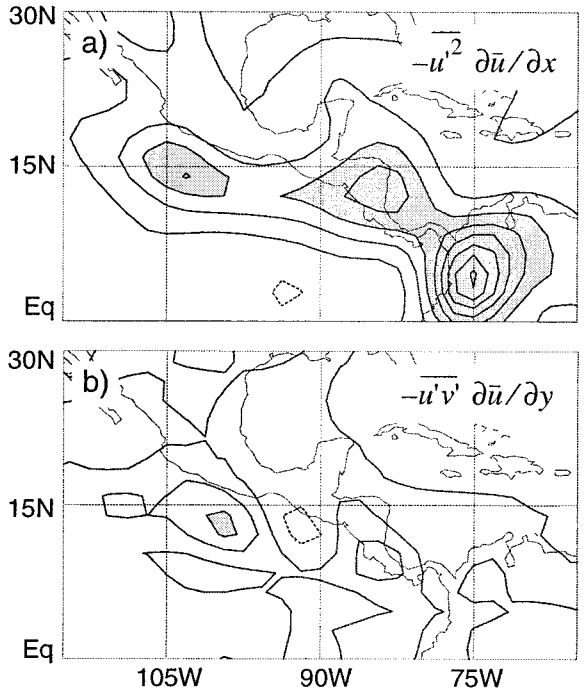

FIG. 4. Simulated barotropic eddy kinetic energy generation by the (a) $-\overline{u'^2}\partial\overline{u}/dx$ and (b) $-\overline{u'v'}\partial\overline{u}/dy$ terms for the positive MJO composite wind field. Otherwise same as Fig. 3c.

winds and forcing, however, because the substantial damping in the model reduces remote influences. We will compare the statistics derived by averaging days 5 to 1000 from model runs with the observed statistics for the composites from 1979–95 shown in Part I. Since the model is linear, the magnitude of the variance is arbitrary. We have scaled the model results by making the model eddy variance maximum for the positive composite similar to that of the observations. This one number is used to scale the negative composite also, so that the differences between the model results for the negative and positive composites result solely from the differences in the background wind field about which the model is linearized.

The model is forced with a randomized source of vorticity with spatially uniform variance as a simple strategy designed to reveal the role of the mean flow structure in producing concentrations of wave energy. The spatial variations in eddy variance that the model produces arise solely from the structure of the mean wind composites. The simulated spatial distributions of eddy energy may differ from those observed for a variety of reasons including the following: 1) where convection occurs it can drive eddy variance and couple the 850-mb vorticity with other levels, 2) the sources of vorticity noise may be inhomogeneous in space, and 3) the vorticity variance may be influenced by topography, which is not included in the model. Nonetheless, the extent to which the model results do resemble observations indicates a strong role for the mean wind structure and barotropic dynamics in organizing the eddy variability.

We begin by comparing the modeled eddy kinetic energy distributions for the positive and negative MJO wind composites for the east Pacific. Figure 3a shows that the eddy kinetic energy has a maximum on the cyclonic and downstream edge of the westerly jet in the positive composite, between 90° and 105°W at about 12°N over the east Pacific. This is in agreement with the observational result shown in Fig. 7 of Part I, although the maximum is displaced a little to the east compared to the observations. For the negative or easterly MJO composite, this east Pacific EKE maximum does not appear (Fig. 3b). The model produces a maximum in eddy energy near the Colombian Andes Mountains, which is not observed. The mean winds converge toward the Andes because of the strong convective heating there, particularly in the positive composite, but in nature strong eddy energies are inhibited by the presence of the topography, which penetrates the 850-mb level. Convection near the Andes is organized by the topography and the diurnal cycle of insolation rather than by eddies. So we can understand why the model produces an EKE maximum near the northern tip of the Andes and why this maximum is not observed in nature. These eddy kinetic energy maxima over the mountains could be reduced by introducing large dissipation where the mountains penetrate the 850-mb surface. We have chosen not to add extra constraints like this to make the simulation more accurate.

In the simulation for the easterly MJO wind composite for the east Pacific, the eddy kinetic energy is greatly reduced compared to the westerly composite (Fig. 3b), in agreement with the observations of Part I. The stochastic barotropic model thus predicts the observed strong localization of eddy kinetic energy near 12°N and between 90° and 105°W, and the much reduced eddy energy in the negative (easterly) phase of the MJO oscillation over the east Pacific. The localization of high eddy energy in the formation region for tropical cyclones can thus be explained at least in part by the interaction of barotropic wave dynamics with the mean wind field.

To better understand the mechanisms of this eddy localization, we will consider the budget for eddy energy in the form used in the observational study of Part I:

$$\frac{\partial K'}{\partial t} = -\overline{\mathbf{V}}\cdot\nabla K' + C(\overline{K}, K') + S, \qquad (6)$$

where K' is the eddy kinetic energy,

$$K' = \frac{1}{2}(\overline{u'^2} + \overline{v'^2}). \qquad (7)$$

The first term on the right is the advection of eddy energy by the mean flow, and the last term is the source term, S, which includes the random forcing and dissi-

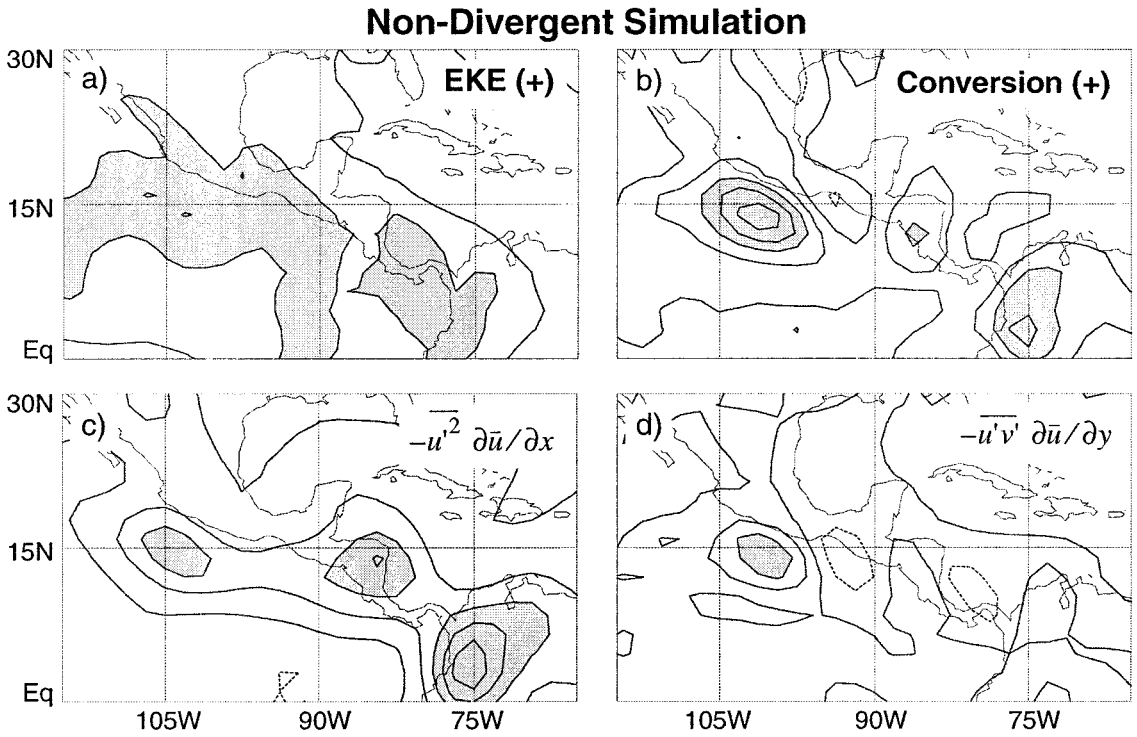

FIG. 5. Simulated (a) eddy kinetic energy and (b) $C(\overline{K}, K')$ for the positive MJO composite case in which only the nondivergent part of the mean wind field is used. Otherwise same as Fig. 3.

pation. The second term on the right is the conversion from mean to eddy kinetic energy:

$$C(\overline{K}, K') = -\overline{u'v'}\left(\frac{\partial\overline{u}}{dy} + \frac{\partial\overline{v}}{dx}\right) - \overline{u'^2}\frac{\partial\overline{u}}{dx} - \overline{v'^2}\frac{\partial\overline{v}}{dy}. \quad (8)$$

For the westerly MJO composite case in both the observations and the model, the largest of four terms in the conversion rate (8) is often the third one one the right, followed in importance by the first.

Rather than the energetic diagnosis we employ here, one could use wave propagation diagnosis, such as the barotropic version of Plumb's (1986) wave activity flux formulation that was applied by Sobel and Bretherton (1999). Indeed the eddy statistics calculated are very similar to those employed by Plumb and in the "**E** Vector" formalism of Hoskins et al. (1983). The wave mean–flow energy exchanges that we describe can thus also be interpreted as the growth of energy that accompanies wave action flux in a spatially varying mean flow. Because of the dominance of the third term in (3), the regions of wave growth that we describe are also related to the ideas of wave accumulation in regions of mean wind convergence that have been explored theoretically in several recent papers (Farrell and Watterson 1985; Webster and Chang 1988; Chang and Webster 1990, 1995).

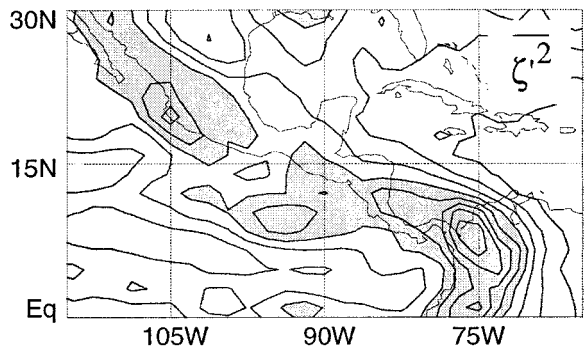

FIG. 6. Simulated eddy vorticity variance for the positive east Pacific MJO composite wind field. Contour interval is 6.0×10^{-11} s^{-2}. Values greater than 3.0×10^{-10} s^{-2} are shaded.

Figures 3c and 3d show the conversion term (8) for the positive and negative composites. In the positive case, the conversion term is large in the region of the east Pacific eddy kinetic energy maximum. Its magnitude is sufficient to replace the mean eddy energy in about a day and a half, much less than the damping time of 5 days, and comparable to the replacement timescale found in the observations. In the negative case the conversion terms are much smaller and no maximum occurs in the east Pacific.

Figure 4 shows the two largest terms in the conversion rate for the positive composite case. The third term in (8) is the largest term and explains the basic shape of the total conversion; the first term on the right in (8) contributes about a third of the total in the east Pacific.

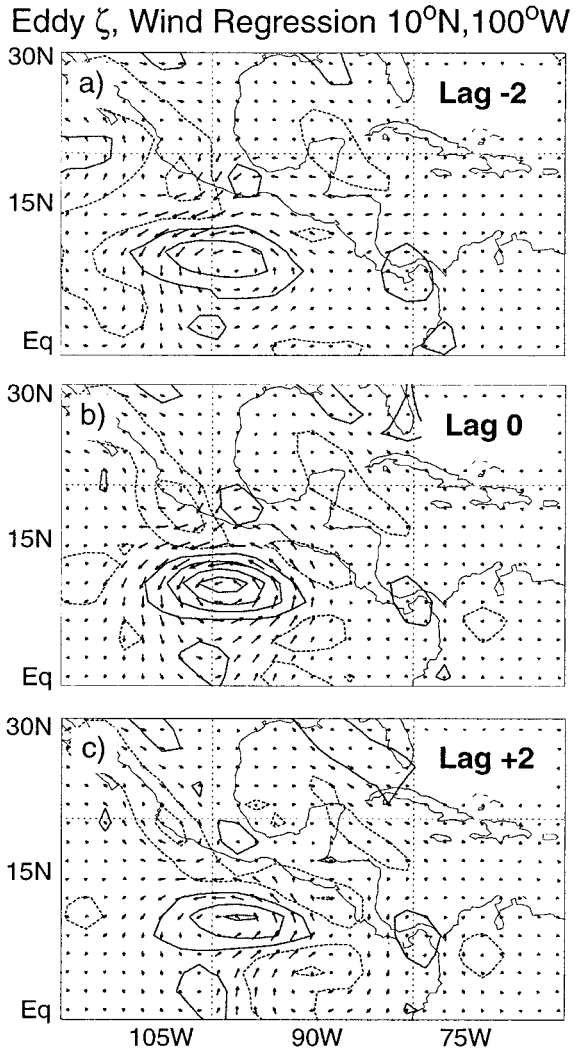

FIG. 7. Regressions of eddy vorticity (contours) and eddy winds on the eddy vorticity time series at 10°N, 100°W for lags of (a) −2, (b) 0, and (c) +2 days, simulated for the positive east Pacific MJO composite winds. Contours are plotted every 4×10^{-6} s^{-1} starting at 2×10^{-6} s^{-1}. The largest wind vector is 3.0 m s^{-1}. Negative contours are dashed.

The first term is related to the meridional sharpness of the jet, as explored in Fig. 2. More of the conversion of mean to eddy energy arises from east–west variations of the mean zonal wind. The structure of the eddy conversion terms is very similar to that observed, as can be seen by comparing Figs. 3 and 4 with Figs. 10 and 11 of Part I.

The winds in the 850-mb composite we used have a divergent component. Holland (1995) and Sobel and Bretherton (1999) both note the potential importance of mean wind convergence in contributing to concentration of eddy energy. To see how important this component is, and how sensitive our model result is to changes in the westerly composite, we repeated the calculation with the divergent component of wind removed. The nondivergent winds were obtained by computing the vorticity from the observed winds and then inverting the vorticity to obtain the rotational component of wind. These winds were then used in the stochastic model in place of the observed winds. The eddy kinetic energy and conversion rates obtained with the nondivergent winds are shown in Fig. 5. The concentration of energy near 12.5°N, 100°W is less pronounced, but still present. The energy conversion is still dominated by the zonal convergence term, even though the total divergence of the mean wind is zero. We conclude that the divergent component of wind is important, but is not essential to the localization of eddy energy in the cyclone formation region. Furthermore, since the advection of eddy energy by the mean flow is a comparatively small term in (6), we conclude that in this case the contribution of the divergent wind to the sharpness of the mean flow structure may be just as important as its convergence.

Vorticity distribution and eddy structure

The distribution of eddy vorticity variance in the westerly composite is shown in Fig. 6. The vorticity variance has a peak near the tropical cyclone formation region, but again the maximum is displaced about 5° to the east of that in the observations shown in Fig. 12 of Part I. The maximum near the coast of Mexico is also displaced eastward and northward, so that it falls over land rather than ocean. These differences may be related to the roles that convection and topography play in nature, which are not included in this simple model. The observed increase of variance over the northern Gulf of Mexico is also not simulated correctly. Eddy kinetic energy generation is weak over the Caribbean in both composites, whereas the observations show an enhancement of EKE in the Caribbean during the westerly phase of the MJO.

Figure 7 shows maps of the lagged regressions of the wind and vorticity fields onto the vorticity at 10°N, 100°W. The eddy structure is elongated in the zonal direction as in the observations of Part I, with strong zonal winds to the north of the vorticity center, but the spatial scale is a little smaller than observed (Fig. 13 of Part I). Another difference is that in the observations the wave moves slowly westward at about 2.5 m s^{-1}, whereas the model eddy is almost stationary. In the model eddy, eastward group velocity is plainly visible in the west to east movement of the largest amplitude winds. In the observations the westward phase propagation is dominant. The modeled structure is clearly Rossby wavelike and the spatial scale is much larger than the dissipation scale of the simulation.

5. West Pacific

We next consider the modeled response to the MJO wind composites in the west Pacific. Figure 8 shows the eddy kinetic energy obtained with spatially uniform

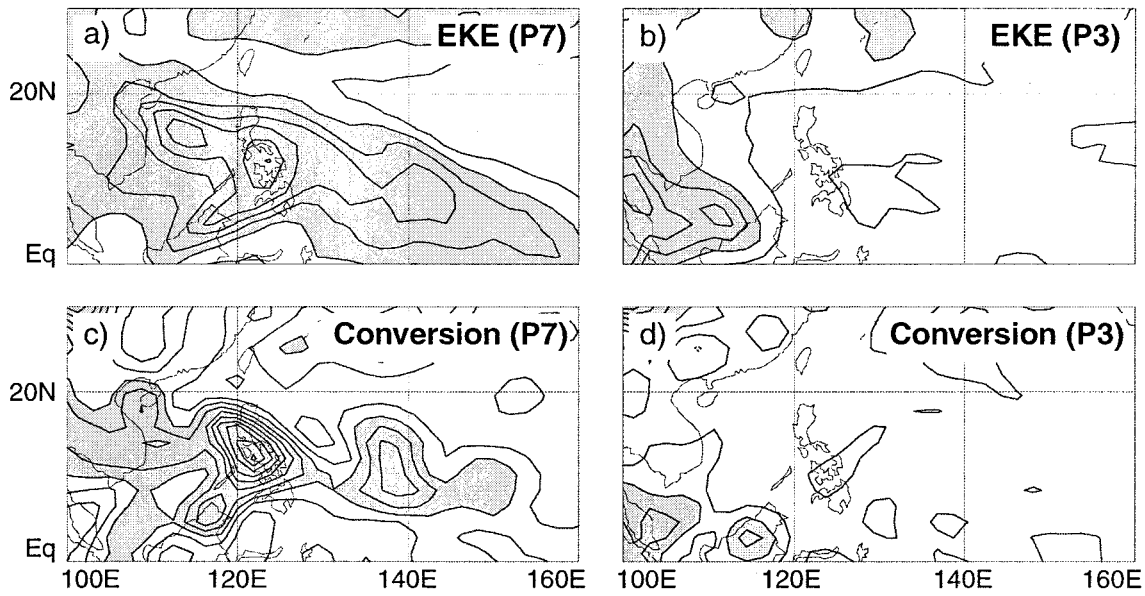

FIG. 8. Simulated 850-mb eddy kinetic energy in the west Pacific for (a) phase 7 and (b) phase 3 MJO composite mean winds. The contour interval is 3 $m^2\ s^{-2}$ and values greater than 12 $m^2\ s^{-2}$ are shaded. Simulated conversion rates for the (c) phase 7 and (d) phase 3 composites. Contour interval is $2.0 \times 10^{-5}\ m^2\ s^{-3}$ and values greater than $4.0 \times 10^{-5}\ m^2\ s^{-3}$ are shaded. Negative contours are dashed.

noise forcing for the westerly (phase 7) and easterly (phase 3) MJO wind composites in the west Pacific shown in Fig. 15 of Part I. For the westerly wind composite, strong maxima in eddy kinetic energy occur to the east and west of the Philippines and extend toward the southeast as in the observations shown in Fig. 16 of Part I. A maximum in eddy kinetic energy directly over the Philippine islands and extending toward Borneo is also simulated, but is not observed. The topography of the Philippines and the island of Borneo may inhibit the growth of synoptic disturbances in those regions. In general, the barotropic model tends to put EKE maxima over land features in the Tropics, where the observations may show a relative minimum. In nature, topography may inhibit the development of synoptic-scale disturbances. The simulation for the westerly MJO phase winds shows much more EKE along the band from the South China Sea toward the east-southeast than for the easterly phase mean winds, in agreement with observations (see Lau and Lau 1990 and Chang et al. 1996, as well as Part I).

Figures 8c and 8d show the total barotropic eddy energy conversion, which has a maxima in the general region of the modeled eddy kinetic energy maxima, with a somewhat larger conversion rate over the Philippine Islands than is observed. The two dominant components

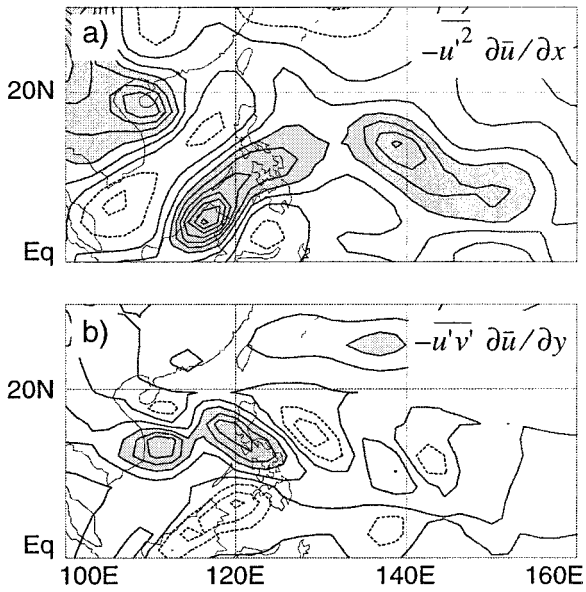

FIG. 9. Simulated barotropic eddy kinetic energy generation by the (a) $-\overline{u'^2}\partial\bar{u}/dx$ and (b) $-\overline{u'v'}\partial\bar{u}/dy$ terms for the phase 7 MJO composite wind field in the west Pacific. Otherwise same as Fig. 8c.

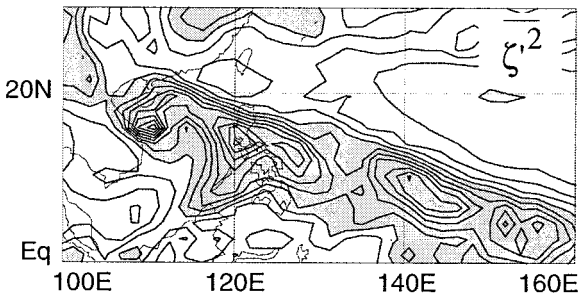

FIG. 10. Simulated eddy vorticity variance for the phase 7 west Pacific MJO composite wind field. Contour interval is $7.0 \times 10^{-11}\ s^{-2}$. Values greater than $4.2 \times 10^{-10}\ s^{-2}$ are shaded.

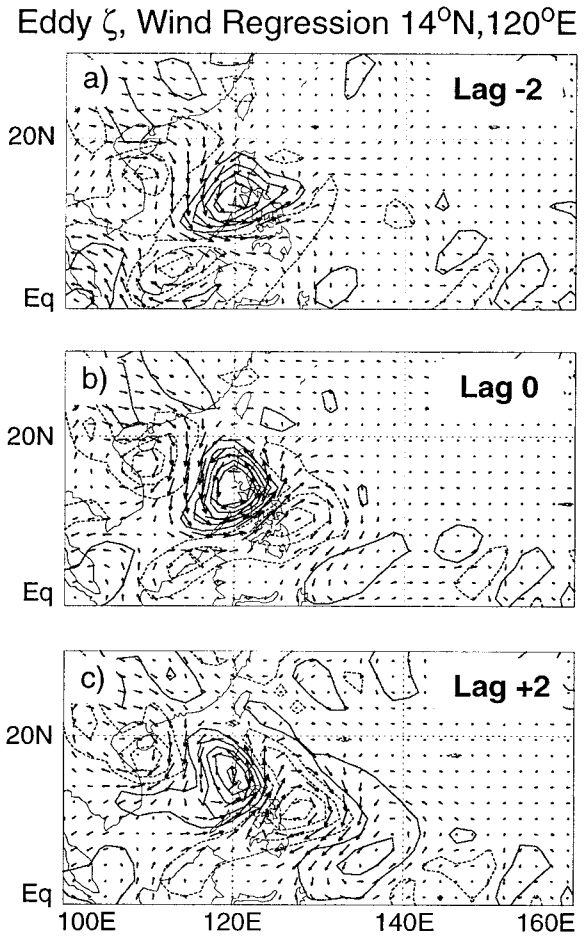

FIG. 11. Regressions of eddy vorticity (contours) and eddy winds on the eddy vorticity time series at 14°N, 120°E for lags of (a) −2, (b) 0, and (c) +2 days, simulated for the positive (phase 7) west Pacific MJO composite winds. Contours are plotted every 4×10^{-6} s^{-1} starting at 2×10^{-6} s^{-1}. The largest wind vector is 4.5 m s^{-1}. Negative contours are dashed.

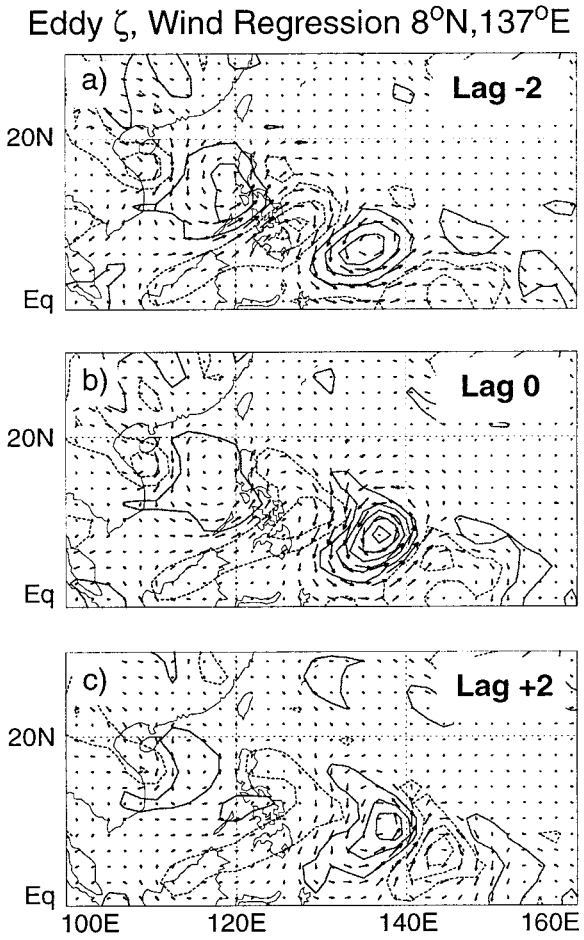

FIG. 12. Same as Fig. 11, but for eddy vorticity time series at 8°N, 137°E. The largest wind vector is 3.0 m s^{-1}. Negative contours are dashed.

of the eddy conversion term are shown in Fig. 9. These are similar in important ways to the observed conversions shown in Fig. 18 of Part I and in Lau and Lau (1992).

The eddy vorticity distribution for the westerly composite (phase 7) is shown in Fig. 10, and is in general agreement with that shown in Fig. 21 of Part I. The extension toward the equator at the date line is particularly well defined. Regression maps about two points along the axis of highest eddy vorticity variance show wave structures that are consistent with short Rossby waves with a wavelength of about 1500 km. Figure 11 shows the lagged regressions of wind and vorticity on vorticity at 14°N, 120°E, and Fig. 12 shows a point farther east and equatorward at 8°N and 137°E. These waves have very small phase speeds and eastward group velocities. The observed eddies are larger in spatial scale, with a wavelength of about 2500 km, and move toward the west. The differences between the eddy structures may be related to the convective heating and the associated stronger connection to upper levels. Although the barotropic model does not predict the observed scale and movement of the eddies, it does correctly predict the location of eddy energy and the effect of the mean winds on the level of eddy activity. The low-level disturbances that the barotropic model predicts are small-scale and slowly moving, which are characteristics that may enable them to serve as seed disturbances that can organize convection and leave to the development of tropical cyclones. The observed regression maps are dominated by mature, energetic systems and it may be unreasonable to expect a barotropic model to reproduce them.

6. Summary and discussion

A stochastic barotropic model forced with spatially uniform vorticity noise can simulate the contrast in eddy kinetic energy between MJO westerly and easterly phases in the eastern and western North Pacific during summer. The maximum in vorticity variance in the region

of tropical cyclone formation, and the general structure of the waves associated with this vorticity variance maximum are both predicted by the model. The eddy kinetic energy maximum is not as strong and isolated as in the observations, however. The eddies are nearly stationary, rather than moving slowly westward as in the observations, and are smaller in spatial scale than the observed eddy structures. These differences in eddy structure are likely to be associated with the effects of convection and vertical shear. The quality of the simulation is impressive considering that latent heat release is not included, and the observed statistics are dominated by disturbances that are heavily influenced by convection. The model thus strongly supports the diagnostic calculations in Part I, which suggest that the response of barotropic processes to the mean flow at 850 mb is a strong control on the provision of seed disturbances that can evolve into tropical cyclones and hurricanes.

The barotropic energy conversions in the stochastic model are similar in structure, mechanism, and intensity to those in the observations. The conversion from mean to eddy energy is dominated by terms associated with zonal gradients in zonal wind, with secondary contributions from meridional eddy momentum transport across latitudinal gradients in zonal wind. In both the observations and the stochastic model, barotropic energy conversions occur at a rate sufficient to replace the local eddy kinetic energy maxima during the active phase in a period of less than two days. During the westerly phase of the MJO the provision of seed disturbances by barotropic processes is collocated with other dynamic and thermodynamic conditions that favor tropical cyclogenesis.

The hypothesis has been made in this paper that interactions between MJO wind variations and eddy energy is most important at low levels where the eddies can easily access the high latent energy of the boundary layer air and lead to the development of tropical cyclones. Once convection starts, however, vertical shear of the mean wind will become important. The implications of this work should therefore be tested with fully three-dimensional calculations. Also, to get a realistic simulation in the region of the tropical Americas, it is undoubtedly necessary to take into account the effect of topography, which was not explicitly considered here.

Acknowledgments. We would like to thank Adam Sobel and Brian Hoskins for helpful conversations early on. George Kiladis, Adrian Matthews, John Molinari, and several anonymous reviewers provided very helpful comments on the manuscript. The Climate Dynamics Program of the National Science Foundation supported this work under Grant ATM-9873691.

REFERENCES

Bourke, W., 1972: An efficient, one-level, primitive-equation spectral model. *Mon. Wea. Rev.,* **100,** 683–689.

Chang, C. P., J. M. Chen, P. A. Harr, and L. E. Carr, 1996: Northwestward-propagating wave patterns over the tropical western North Pacific during summer. *Mon. Wea. Rev.*, **124,** 2245–2266.

Chang, H. R., and P. J. Webster, 1990: Energy accumulation and emanation at low latitudes. Part II: Nonlinear response to strong episodic equatorial forcing. *J. Atmos. Sci.,* **47,** 2624–2644.

——, and ——, 1995: Energy accumulation and emanation at low latitudes. Part III: Forward and backward accumulation. *J. Atmos. Sci.,* **52,** 2384–2403.

Charney, J. G., 1963: A note on the large-scale motions in the tropics. *J. Atmos. Sci.,* **20,** 607–609.

Davidson, N. E., and H. H. Hendon, 1989: Downstream development in the Southern Hemisphere monsoon during FGGE/WMONEX. *Mon. Wea. Rev.*, **117,** 1458–1470.

Egger, J., and H. D. Schilling, 1984: Stochastic forcing of planetary scale flow. *J. Atmos. Sci.,* **41,** 779–788.

Farrell, B., and I. Watterson, 1985: Rossby waves in opposing currents. *J. Atmos. Sci.,* **42,** 1746–1756.

——, and P. J. Ioannou, 1993: Stochastic forcing of the linearized Navier–Stokes equations. *Phys. Fluids A,* **5,** 2600–2609.

——, and ——, 1994: A theory for the statistical equilibrium energy spectrum and heat flux produced by transient baroclinic waves. *J. Atmos. Sci.,* **51,** 2685–2698.

Gambo, K., 1982: Vorticity equation of transient ultra-long waves in middle latitudes in winter regarded as Langevin's equation in Brownian motion. *J. Meteor. Soc. Japan,* **60,** 206–214.

Gray, W. M., 1998: The formation of tropical cyclones. *Meteor. Atmos. Phys.,* **67,** 37–69.

Holland, G. J., 1995: Scale interaction in the western Pacific monsoon. *Meteor. Atmos. Phys.,* **56,** 1–2.

Holton, J. R., 1992: *An Introduction to Dynamic Meteorology.* 3d ed. Academic Press, 511 pp.

Hoskins, B. J., I. N. James, and G. H. White, 1983: The shape, propagation and mean-flow interaction of large-scale weather systems. *J. Atmos. Sci.,* **40,** 1595–1612.

Lau, K.-H., and N.-C. Lau, 1990: Observed structure and propagation characteristics of tropical summertime synoptic scale disturbances. *Mon. Wea. Rev.,* **118,** 1888–1913.

——, and ——, 1992: The energetics and propagation dynamics of tropical summertime synoptic-scale disturbances. *Mon. Wea. Rev.,* **120,** 2523–2539.

Liebmann, B., H. H. Hendon, and J. D. Glick, 1994: The relationship between tropical cyclones of the western Pacific and Indian Oceans and the Madden–Julian oscillation. *J. Meteor. Soc. Japan,* **72,** 401–411.

Maloney, E. D., and D. L. Hartmann, 2000: Modulation of eastern North Pacific Hurricanes by the Madden–Julian oscillation. *J. Climate,* **13,** 1451–1460.

——, and ——, 2001: The Madden–Julian oscillation, Barotropic dynamics, and North Pacific tropical cyclone formation. Part I: Observations. *J. Atmos. Sci.*, **58,** 2545–2558.

Metz, W., 1987: Transient eddy forcing of low-frequency atmospheric variability. *J. Atmos. Sci.,* **44,** 2407–2417.

Nakazawa, T., 1986: Mean features of 30–60-day variations as inferred from 8-year OLF data. *J. Meteor. Soc. Japan,* **64,** 777–786.

Newman, M., P. D. Sardeshmukh, and C. Penland, 1997: Stochastic forcing of the wintertime extratropical flow. *J. Atmos. Sci.,* **54,** 435–455.

Nieto-Ferreira, R., and W. H. Schubert, 1997: Barotropic aspects of ITCZ breakdown. *J. Atmos. Sci.,* **54,** 261–285.

Penland, C., and L. Matrosova, 1994: A balance condition for stochastic numerical models with application to the El Niño–Southern Oscillation. *J. Climate,* **7,** 1352–1372.

Plumb, A. R., 1986: Three-dimensional propagation of transient quasi-geostrophic eddies and its relation with the eddy forcing of the time-mean flow. *J. Atmos. Sci.,* **43,** 1657–1670.

Reed, R. J., and R. H. Johnson, 1974: The vorticity budget of synoptic-scale wave disturbances in the tropical western Pacific. *J. Atmos. Sci.,* **31,** 1784–1790.

Sardeshmukh, P. D., and B. J. Hoskins, 1988: The generation of global rotational flow by steady idealized tropical divergence. *J. Atmos. Sci.,* **45,** 1228–1251.

Shapiro, L. J., 1978: The vorticity budget of a composite African Wave. *Mon. Wea. Rev.,* **106,** 806–817.

Sobel, A. H., and C. S. Bretherton, 1999: Development of synoptic-scale disturbances over the summertime tropical northwest Pacific. *J. Atmos. Sci.,* **56,** 3106–3127.

——, and E. D. Maloney, 2000: Effect of ENSO and the MJO on western North Pacific tropical cyclones. *Geophys. Res. Lett.,* **27,** 1739–1742.

Stevens, D. E., 1979: Vorticity, momentum, and divergence budgets of synoptic-scale wave disturbances in the tropical eastern Atlantic. *Mon. Wea. Rev.,* **107,** 535–550.

Webster, P. J., and H. R. Chang, 1988: Equatorial energy accumulation and emanation regions: impact of a zonally varying basic state. *J. Atmos. Sci.,* **45,** 803–829.

Whitaker, J. S., and P. D. Sardeshmukh, 1998: A linear theory of extratropical synoptic eddy statistics. *J. Atmos. Sci.,* **55,** 237–258.

Zehr, R. M., 1992: Tropical cyclogenesis in the western North Pacific. NOAA Tech. Rep. NESDIS 61, 181 pp. [Available from U.S. Department of Commerce, NOAA/NESDIS, 5200 Auth Rd., Washington, D.C. 20233.]